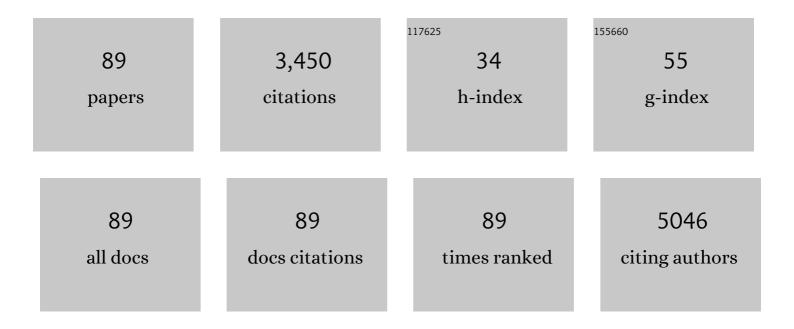
Yucheng Wu

List of Publications by Year in descending order

Source: https://exaly.com/author-pdf/9579683/publications.pdf Version: 2024-02-01



<u> Үнснемс Ми</u>

#	Article	IF	CITATIONS
1	Highly efficient solar-driven photocatalytic hydrogen evolution with FeMoSx/mpg-C3N4 heterostructure. Chemical Engineering Journal, 2022, 427, 131507.	12.7	4
2	ZIF-8 derived TiO2/ZnO heterostructure decorated with AgNPs as SERS sensor for sensitive identification of trace pesticides. Journal of Alloys and Compounds, 2022, 901, 163675.	5.5	19
3	Al doped Ni-Co layered double hydroxides with surface-sulphuration for highly stable flexible supercapacitors. Journal of Colloid and Interface Science, 2022, 615, 173-183.	9.4	19
4	A Highâ€Efficiency Mo ₂ C Electrocatalyst Promoting the Polysulfide Redox Kinetics for Na–S Batteries. Advanced Materials, 2022, 34, e2200479.	21.0	72
5	Layer-by-Layer Assembly of CeO _{2–<i>x</i>} @C-rGO Nanocomposites and CNTs as a Multifunctional Separator Coating for Highly Stable Lithium–Sulfur Batteries. ACS Applied Materials & Interfaces, 2022, 14, 18634-18645.	8.0	24
6	In situ W/O Co-doped hollow carbon nitride tubular structures with enhanced visible-light-driven photocatalytic performance for hydrogen evolution. International Journal of Hydrogen Energy, 2021, 46, 234-246.	7.1	19
7	Theoretical understanding for anchoring effect of MOFs for lithium-sulfur batteries. Computational and Theoretical Chemistry, 2021, 1196, 113110.	2.5	4
8	Controlled growth of porous oxygen-deficient NiCo ₂ O ₄ nanobelts as high-efficiency electrocatalysts for oxygen evolution reaction. Catalysis Science and Technology, 2021, 11, 264-271.	4.1	11
9	Carbon Nanolayer-Wrapped Mesoporous TiO ₂ –B/Anatase for Li ⁺ Storage. ACS Applied Nano Materials, 2021, 4, 7832-7839.	5.0	8
10	Lightâ€Driven Selfâ€Oscillating Actuators with Phototactic Locomotion Based on Black Phosphorus Heterostructure. Angewandte Chemie, 2021, 133, 20674-20680.	2.0	3
11	Lightâ€Driven Selfâ€Oscillating Actuators with Phototactic Locomotion Based on Black Phosphorus Heterostructure. Angewandte Chemie - International Edition, 2021, 60, 20511-20517.	13.8	82
12	3D Tungsten Disulfide/Carbon Nanotube Networks as Separator Coatings and Cathode Additives for Stable and Fast Lithium–Sulfur Batteries. ACS Applied Materials & Interfaces, 2021, 13, 45547-45557.	8.0	17
13	New insights into synergistic effects of La2O3 and nitrogen doped carbon for improved redox kinetics in lithium-sulfur batteries: A computational study. Applied Surface Science, 2021, 563, 150172.	6.1	10
14	Ag Nanoparticle-Decorated Mesoporous Silica as a Dual-Mode Raman Sensing Platform for Detection of Volatile Organic Compounds. ACS Applied Nano Materials, 2021, 4, 1019-1028.	5.0	13
15	Improved hydrogen evolution with SnS ₂ quantum dot-incorporated black Si photocathode. Dalton Transactions, 2021, 50, 13329-13336.	3.3	3
16	Designing core–shell metal–organic framework hybrids: toward high-efficiency electrochemical potassium storage. Journal of Materials Chemistry A, 2021, 9, 26181-26188.	10.3	10
17	3D Hierarchical Urchin-Like Ni _{0.3} Co _{0.6} Cu _{0.1} (CO ₃) _{0.5} (OH) Microspheres for Supercapacitors with High Specific Capacitance. Energy & Fuels, 2021, 35, 20358-20366.	5.1	11
18	Rational Design of Nanostructured Electrode Materials toward Multifunctional Supercapacitors. Advanced Functional Materials, 2020, 30, 1902564.	14.9	252

#	Article	IF	CITATIONS
19	Fabrication of WO3/TiO2 core-shell nanowire arrays: Structure design and high electrochromic performance. Electrochimica Acta, 2020, 330, 135189.	5.2	34
20	A surface precleaning strategy intensifies the interface coupling of the Bi ₂ O ₃ /TiO ₂ heterostructure for enhanced photoelectrochemical detection properties. Materials Chemistry Frontiers, 2020, 4, 638-644.	5.9	9
21	Synthesis of SrTiO ₃ submicron cubes with simultaneous and competitive photocatalytic activity for H ₂ O splitting and CO ₂ reduction. RSC Advances, 2020, 10, 42619-42627.	3.6	10
22	Rational construction of porous amorphous WO3 nanostructures with high electrochromic energy storage performance: Effect of temperature. Journal of Non-Crystalline Solids, 2020, 549, 120337.	3.1	12
23	Theoretical Insights into the Favorable Functionalized Ti ₂ C-Based MXenes for Lithium–Sulfur Batteries. ACS Omega, 2020, 5, 29272-29283.	3.5	28
24	Rational Regulation of Surface Free Radicals on TiO2 Nanotube Arrays via Ag2O–AgBiO3 towards Enhanced Selective Photoelectrochemical Detection. Nanomaterials, 2020, 10, 2002.	4.1	1
25	Enhanced Energy Storage Performance of 3D Hybrid Metal Sulfides via Synergistic Engineering of Architecture and Composition. ACS Sustainable Chemistry and Engineering, 2020, 8, 11491-11500.	6.7	5
26	A multifunctional separator based on scandium oxide nanocrystal decorated carbon nanotubes for high performance lithium–sulfur batteries. Nanoscale, 2020, 12, 6832-6843.	5.6	34
27	Rational Design of Oxygen Deficiency-Controlled Tungsten Oxide Electrochromic Films with an Exceptional Memory Effect. ACS Applied Materials & Interfaces, 2020, 12, 32658-32665.	8.0	46
28	Theoretical prediction of B/Al-doped black phosphorus as potential cathode material in lithium-sulfur batteries. Applied Surface Science, 2020, 512, 145639.	6.1	22
29	Assembling of Bi atoms on TiO ₂ nanorods boosts photoelectrochemical water splitting of semiconductors. Nanoscale, 2020, 12, 4302-4308.	5.6	49
30	Solution synthesis ultrathin PbTe0.5Se0.5 nanowires and the low lattice thermal conductivity. Journal of Physics and Chemistry of Solids, 2020, 141, 109370.	4.0	3
31	Ni–Co coordination hollow spheres for high performance flexible all-solid-state supercapacitor. Electrochimica Acta, 2020, 337, 135828.	5.2	27
32	Structure modulated amorphous/crystalline WO3 nanoporous arrays with superior electrochromic energy storage performance. Solar Energy Materials and Solar Cells, 2020, 212, 110579.	6.2	45
33	Plasmon-coupled 3D porous hotspot architecture for super-sensitive quantitative SERS sensing of toxic substances on real sample surfaces. Physical Chemistry Chemical Physics, 2019, 21, 19288-19297.	2.8	12
34	Local nanostructures enhanced the thermoelectric performance of n-type PbTe. Journal of Materials Chemistry A, 2019, 7, 18458-18467.	10.3	53
35	Mechanistic Insights into the Chemo- and Regio-Selective B(C6F5)3 Catalyzed C–H Functionalization of Phenols with Diazoesters. Journal of Organic Chemistry, 2019, 84, 14508-14519.	3.2	27
36	Construction of WO3/Ti-doped WO3 bi-layer nanopore arrays with superior electrochromic and capacitive performances. Tungsten, 2019, 1, 236-244.	4.8	7

#	Article	IF	CITATIONS
37	Crystalline WO3 nanowires array sheathed with sputtered amorphous shells for enhanced electrochromic performance. Applied Surface Science, 2019, 498, 143796.	6.1	42
38	MoS <i>_x</i> Quantum Dot-Modified Black Silicon for Highly Efficient Photoelectrochemical Hydrogen Evolution. ACS Sustainable Chemistry and Engineering, 2019, 7, 17598-17605.	6.7	17
39	Coordination derived stable Ni–Co MOFs for foldable all-solid-state supercapacitors with high specific energy. Journal of Materials Chemistry A, 2019, 7, 4998-5008.	10.3	133
40	Inorganic CsBi ₃ I ₁₀ perovskite/silicon heterojunctions for sensitive, self-driven and air-stable NIR photodetectors. Journal of Materials Chemistry C, 2019, 7, 863-870.	5.5	50
41	A bioinspired multi-functional wearable sensor with an integrated light-induced actuator based on an asymmetric graphene composite film. Journal of Materials Chemistry C, 2019, 7, 6879-6888.	5.5	42
42	Highly Efficient Photoinduced Enhanced Raman Spectroscopy (PIERS) from Plasmonic Nanoparticles Decorated 3D Semiconductor Arrays for Ultrasensitive, Portable, and Recyclable Detection of Organic Pollutants. ACS Sensors, 2019, 4, 1670-1681.	7.8	50
43	An amorphous MoSx modified g-C3N4 composite for efficient photocatalytic hydrogen evolution under visible light. RSC Advances, 2019, 9, 15900-15909.	3.6	20
44	Nitrogen, sulfur-codoped micro–mesoporous carbon derived from boat-fruited sterculia seed for robust lithium–sulfur batteries. RSC Advances, 2019, 9, 15715-15726.	3.6	24
45	Sulfur-deficient MoS2-x promoted lithium polysulfides conversion in lithium-sulfur battery: A first-principles study. Applied Surface Science, 2019, 487, 452-463.	6.1	58
46	Dithiothreitol-assisted polysulfide reduction in the interlayer of lithium–sulfur batteries: a first-principles study. Physical Chemistry Chemical Physics, 2019, 21, 16435-16443.	2.8	7
47	Systematic study on hybrid supercapacitor of Ni-Co layered double hydroxide//activated carbons. Electrochimica Acta, 2019, 305, 403-415.	5.2	58
48	Z-scheme carbon-bridged Bi2O3/TiO2 nanotube arrays to boost photoelectrochemical detection performance. Applied Catalysis B: Environmental, 2019, 248, 255-263.	20.2	85
49	Hollow Au nanorattles for boosting the performance of organic photovoltaics. Journal of Materials Chemistry A, 2019, 7, 26797-26803.	10.3	11
50	Ultrafast, Self-Driven, and Air-Stable Photodetectors Based on Multilayer PtSe ₂ /Perovskite Heterojunctions. Journal of Physical Chemistry Letters, 2018, 9, 1185-1194.	4.6	159
51	Photo-assisted synthesis of coaxial-structured polypyrrole/electrochemically hydrogenated TiO2 nanotube arrays as a high performance supercapacitor electrode. RSC Advances, 2018, 8, 13393-13400.	3.6	10
52	Anti-site defect effect on the electronic structure of a Bi ₂ Te ₃ topological insulator. RSC Advances, 2018, 8, 423-428.	3.6	42
53	Thermal shock behavior of W–ZrC/Sc2O3 composites under two different transient events by electron and laser irradiation. Journal of Nuclear Materials, 2018, 499, 248-255.	2.7	10
54	Biomimetic synthesis of hierarchical 3D Ag butterfly wing scale arrays/graphene composites as ultrasensitive SERS substrates for efficient trace chemical detection. Journal of Materials Chemistry C, 2018, 6, 1933-1943.	5.5	39

#	Article	IF	CITATIONS
55	Synthesis of alloyed Zn _{1–x} Mn _x S nanowires with completely controlled compositions and tunable bandgaps. RSC Advances, 2018, 8, 374-379.	3.6	14
56	<i>In situ</i> growth of PEDOT/graphene oxide nanostructures with enhanced electrochromic performance. RSC Advances, 2018, 8, 13679-13685.	3.6	41
57	Ni(OH) ₂ /CNTs hierarchical spheres for a foldable all-solid-state supercapacitor with high specific energy. Nanoscale, 2018, 10, 7377-7381.	5.6	52
58	MOF-74 derived porous hybrid metal oxide hollow nanowires for high-performance electrochemical energy storage. Journal of Materials Chemistry A, 2018, 6, 8396-8404.	10.3	101
59	CeO _{2â^'x} /C/rGO nanocomposites derived from Ce-MOF and graphene oxide as a robust platform for highly sensitive uric acid detection. Nanoscale, 2018, 10, 1939-1945.	5.6	88
60	Preparation of V ₂ O ₅ dot-decorated WO ₃ nanorod arrays for high performance multi-color electrochromic devices. Journal of Materials Chemistry C, 2018, 6, 12206-12216.	5.5	31
61	Plasmonic 3D Semiconductor–Metal Nanopore Arrays for Reliable Surface-Enhanced Raman Scattering Detection and In-Site Catalytic Reaction Monitoring. ACS Sensors, 2018, 3, 2446-2454.	7.8	36
62	Mesoporous anodic α-Fe2O3 interferometer for organic vapor sensing application. RSC Advances, 2018, 8, 31121-31128.	3.6	10
63	Rationally Designed Graphene/Bilayer Silver/Cu Hybrid Structure with Improved Sensitivity and Stability for Highly Efficient SERS Sensing. ACS Omega, 2018, 3, 5761-5770.	3.5	11
64	Crystalline orientation preference for TiO2 nanotube arrays with efficient photoelectrochemical properties. Physics Letters, Section A: General, Atomic and Solid State Physics, 2018, 382, 2759-2762.	2.1	16
65	Electrically and Sunlightâ€Driven Actuator with Versatile Biomimetic Motions Based on Rolled Carbon Nanotube Bilayer Composite. Advanced Functional Materials, 2017, 27, 1704388.	14.9	211
66	Synthesis of α-Bi ₂ Mo ₃ O ₁₂ /TiO ₂ Nanotube Arrays for Photoelectrochemical COD Detection Application. Langmuir, 2017, 33, 8933-8942.	3.5	27
67	Electrochemical hydrogenated TiO ₂ nanotube arrays decorated with 3D cotton-like porous MnO ₂ enables superior supercapacitive performance. RSC Advances, 2017, 7, 31512-31518.	3.6	6
68	Remarkable supercapacitive performance of TiO2 nanotube arrays by introduction of oxygen vacancies. Chemical Engineering Journal, 2017, 313, 1071-1081.	12.7	64
69	Supercapacitive performance of homogeneous Co3O4/TiO2 nanotube arrays enhanced by carbon layer and oxygen vacancies. Journal of Solid State Electrochemistry, 2017, 21, 1069-1078.	2.5	17
70	Graphitic carbon nitride nanosheets obtained by liquid stripping as efficient photocatalysts under visible light. RSC Advances, 2017, 7, 37185-37193.	3.6	68
71	One-step electrodeposition of Co 0·12 Ni 1·88 S 2 @Co 8 S 9 nanoparticles on highly conductive TiO 2 nanotube arrays for battery-type electrodes with enhanced energy storage performance. Journal of Power Sources, 2017, 364, 400-409.	7.8	17
72	Photoelectrochemical detection performance and mechanism discussion of Bi ₂ O ₃ modified TiO ₂ nanotube arrays. RSC Advances, 2016, 6, 61367-61377.	3.6	14

#	Article	IF	CITATIONS
73	Supercapacitive performance of electrochemically doped TiO ₂ nanotube arrays decorated with Cu ₂ O nanoparticles. RSC Advances, 2016, 6, 47669-47675.	3.6	14
74	Integration of mesoporous nickel cobalt oxide nanosheets with ultrathin layer carbon wrapped TiO ₂ nanotube arrays for high-performance supercapacitors. New Journal of Chemistry, 2016, 40, 6881-6889.	2.8	18
75	All solid supercapacitors based on an anion conducting polymer electrolyte. RSC Advances, 2016, 6, 19826-19832.	3.6	17
76	Synthesis of porous NiO/CeO ₂ hybrid nanoflake arrays as a platform for electrochemical biosensing. Nanoscale, 2016, 8, 770-774.	5.6	41
77	Electrochemical Biosensor based on Pt/Au Alloy Nanowire Arrays for Phosphate Detection. Journal of the Electrochemical Society, 2015, 162, B62-B67.	2.9	34
78	Photocatalytic property of a Bi ₂ O ₃ nanoparticle modified BiOCl composite with a nanolayered hierarchical structure synthesized by in situ reactions. Dalton Transactions, 2015, 44, 5386-5395.	3.3	38
79	A facile synthesis of mesoporous Co ₃ O ₄ /CeO ₂ hybrid nanowire arrays for high performance supercapacitors. Journal of Materials Chemistry A, 2015, 3, 10425-10431.	10.3	108
80	Photoelectrochemical properties and the detection mechanism of Bi ₂ WO ₆ nanosheet modified TiO ₂ nanotube arrays. Dalton Transactions, 2015, 44, 17784-17794.	3.3	16
81	Integration of a highly ordered gold nanowires array with glucose oxidase for ultra-sensitive glucose detection. Analytica Chimica Acta, 2014, 809, 134-140.	5.4	37
82	Core–Shell Heterojunction of Silicon Nanowire Arrays and Carbon Quantum Dots for Photovoltaic Devices and Self-Driven Photodetectors. ACS Nano, 2014, 8, 4015-4022.	14.6	258
83	Photoelectrochemical Performances and Potential Applications of TiO2 Nanotube Arrays Modified with Ag and Pt Nanoparticles. Electrochimica Acta, 2014, 121, 194-202.	5.2	41
84	A flake-tube structured BiOBr–TiO ₂ nanotube array heterojunction with enhanced visible light photocatalytic activity. New Journal of Chemistry, 2014, 38, 3022-3028.	2.8	38
85	Flow-through TiO2 nanotube arrays: a modified support with homogeneous distribution of Ag nanoparticles and their photocatalytic activities. New Journal of Chemistry, 2013, 37, 752.	2.8	19
86	Perovskite Chromates Cathode with Exsolved Iron Nanoparticles for Direct High-Temperature Steam Electrolysis. ACS Applied Materials & amp; Interfaces, 2013, 5, 8553-8562.	8.0	49
87	Photoluminescence properties of Eu3+ and Bi3+ in YBO3 host under vacuum ultraviolet/ultraviolet excitation. Journal of Applied Physics, 2009, 105, 013513.	2.5	31
88	Composition Dependent Magnetic Properties of Ni-Co-P Coated Carbon Nanotubes. Chinese Journal of Chemical Physics, 2009, 22, 411-416.	1.3	4
89	Porous Copper Foamâ€based Plasmonic Nanocrystals Modified Threeâ€dimensional Semiconductor Nanoflowers for Multifold, Recyclable and Portable Detection of Environmental Contaminant. Particle and Particle Systems Characterization, 0, , 2200072.	2.3	1